

Short Report

Yttrium mapping on fossil teeth by micro-XRF for apatite U–Pb dating

Kazumasa AOKI[1*], Kentaro CHIBA[2], Tetsu KOGISO[3], Kaisei MURAKAMI[2] & Khishigjav TSOGTBAATAR[4]

Abstract: Selecting appropriate measurement points is crucial for apatite U–Pb dating of fossil teeth due to the impact of post-fossilization alterations. Previous studies have suggested that variations in yttrium (Y) concentrations within each sample can be qualitative indicators of such alterations (Y-screening method). To verify the validity of this method, ideal measurement areas for U–Pb dating were selected from Y mapping using a micro-focus X-ray fluorescence spectrometer (micro-XRF) on Late Cretaceous *Tarbosaurus* teeth with published apatite U–Pb ages, and trace element analysis and U–Pb dating of apatite was performed by laser ablation and inductively coupled plasma mass spectrometry (LA-ICP-MS). Two ages of 64.3 ± 3.4 Ma and 61.0 ± 11.0 Ma were obtained from two regions of relatively different Y concentrations in a sample that had been reported as 66.7 ± 2.5 Ma. Similarly, the sample with the reported age of approximately 30 Ma yielded ages of 51.5 ± 2.7 Ma and 57.3 ± 6.1 Ma in the areas with relatively low Y concentrations. These results show that Y concentration and an apatite U–Pb age are correlated, at least within the same sample, and support the usefulness of the Y-screening method. Although more measurements are needed to obtain conclusive proof, the Y micro-XRF mapping would be a helpful tool for non-destructive visualization of post-fossilization alteration in tooth fossils and could lead to the selection of suitable measuring points for LA-ICP-MS apatite U–Pb dating.

I. Introduction

The lack of a rigorous temporal framework for certain strata is often a barrier to elucidating the evolutionary history of organisms in the fossil record. Recently, the uranium–lead (U–Pb) dating of calcites in caliches and apatites from teeth has attracted attention as a valuable technique to constrain the temporal range of fossil-bearing strata (e.g., Fassett et al. 2011, Greene et al. 2018, Kurumada et al. 2020, Barreto et al. 2022, Tanabe et al. 2023). However, one major concern of this technique, especially when applied to tooth fossils, is its susceptibility to post-fossilization. Occasionally, the obtained apatite U–Pb ages of teeth are affected by secondary redistribution of U and common Pb contamination and may not always directly represent the depositional ages of fossil-bearing strata (e.g., Romer 2001, Kocsis et al. 2010, Greene et al. 2018). Previous studies have reported that the differences in yttrium (Y) concentration within a sample can serve as a proxy for post-fossilization alterations (Y-screening method) and the effect of alteration manifesting as the rejuvenation of the fossilization age (Greene et al. 2018, Tanabe et al. 2023). In this study, therefore, we combined Y mapping using a microfocus X-ray fluorescence spectrometer (micro-XRF) with U–Pb dating and trace element analysis of two *Tarbosaurus bataar* teeth performed by laser ablation inductively coupled plasma mass spectrometry (LA-ICP-MS) to validate the efficacy of this screening method. We would like to report it here as a short communication and emphasize the usefulness of Y micro-XRF mapping for non-destructive visualization of post-fossilization alterations in fossil teeth and for the selection of optimal measuring points for LA-ICP-MS apatite U–Pb dating.

II. Samples

The joint expedition of Okayama University of Science and the Institute of Paleontology, Mongolian Academy of Science was conducted at Bugin Tsav in the Gobi Desert, Mongolia in 2018 (Ishigaki et al. 2018; Fig. 1). In this locality, the middle Nemegt Formation is exposed (Jerzykiewicz & Russell 1991, Eberth 2018). The depositional age of this formation is poorly

[1.] Center for Fundamental Education, Okayama University of Science, 1-1 Ridai-cho, Kita-ku, Okayama-shi, Okayama 700-0005, Japan. 岡山理科大学教育推進機構基盤教育センター, 〒700-0005 岡山県岡山市北区理大町1-1.
[2.] Department of Biosphere-Geosphere Science, Faculty of Biosphere-Geosphere Science, Okayama University of Science, 1-1 Ridai-cho, Kita-ku, Okayama-shi, Okayama 700-0005, Japan. 岡山理科大学生物地球学部生物地球学科, 〒700-0005 岡山県岡山市北区理大町1-1.
[3.] Graduate School of Human and Environmental Studies, Kyoto University, Yoshidanihommatsu-cho, Sakyo-ku, Kyoto-shi, Kyoto 606-8501, Japan. 京都大学大学院人間・環境学研究科, 〒606-8501 京都府京都市左京区吉田二本松町.
[4.] Institute of Paleontology, Mongolian Academy of Sciences, Ulaanbaatar 14200, Mongolia. モンゴル科学アカデミー古生物学研究センター, 〒14200 モンゴル国ウランバートル.
*Correspondence: Kazumasa AOKI, E-mail: kazumasa@ous.ac.jp

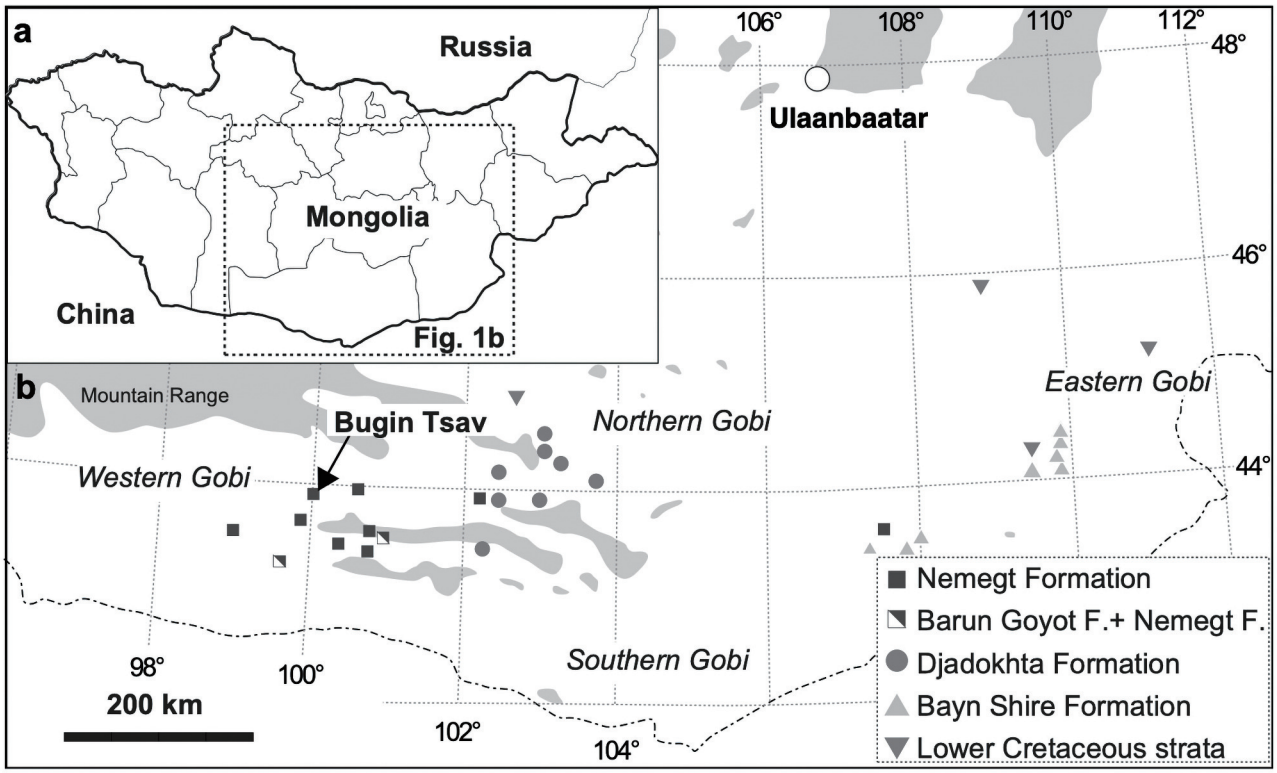

Fig. 1. Geological map of Mongolia. (a) Simplified map of Mongolia with the surrounding countries. (b) Location of Cretaceous formational outcrops in the Gobi Desert. Locations of the Bugin Tsav in the Nemegt Basin are also shown (Tanabe et al. 2023).

constrained due to the lack of igneous rocks available for absolute dating (Shuvalov 2000) and the endemicity of the fossil assemblage (Jerzykiewicz & Russell 1991), but generally thought to be late Campanian to Maastrichtian based on faunal comparisons (e.g., Jerzykiewicz & Russell 1991, Khand et al. 2000). Recently, Tanabe et al. (2023) reported apatite U–Pb ages using the teeth of a large theropod dinosaur *Tarbosaurus*, collected at Bugin Tsav during the expedition, which supports the previously suggested relative age of the formation. We used two of the specimens in Tanabe et al. (2023) for further analyses in this study: MPC-D 100s/002 (Fig. 2a) and MPC-D 100s/003 (Fig. 2b). Further details of the samples are given in Tanabe et al. (2023).

III. Analytical Method

The Y-mapping analyses were conducted using an energy-dispersive X-ray spectrometer (EDS) attached to a micro-XRF (XGT7000V; Horiba, Kyoto, Japan) at Kyoto University. A tube voltage of 50 kV, a tube current of 1.0 mA, and an X-ray beam of 100 μm in vacuo was used for the analysis. The samples were scanned in approximately 34 and 50 μm intervals (pixel size) depending on the range of the sample size. The intensity of Y was determined from the cumulative intensity of the repeated analyses (up to four times). The analysis of the elemental maps was conducted using the Image J program (https://imagej.net/ij/index.html). Further details of the micro-XRF analysis method are given in Machida et al. (2021).

In-situ trace element analyses of the fossil teeth were performed with an iCAP-RQ single-collector quadrupole ICP-MS (Thermo Scientific, USA) coupled to an ArF Excimer Laser Analyte G2 (Teledyne-Photon Machines, USA) at Okayama University of Science (OUS). The laser was operated with a repetition rate of 5 Hz and a laser spot diameter of 35 μm, which provided an estimated power density of the sample of 1.72 J/cm^2. The pulse count was 150 shots. After shooting with the shutter closed for 30 s while the laser warmed up, the analytical areas were ablated for 30 s. Prior to conducting the analysis, the analyzed spots were ablated using a pulse of the laser with a diameter of 50 μm to remove potential contaminants on their surfaces. The ICP-MS was optimized using continuous ablation of a NIST SRM 612 glass standard to provide maximum sensitivity while maintaining low oxide formation ($^{232}Th^{16}O/^{232}Th < 1\%$). ^{43}Ca was used as an internal standard element. In this study, the Y of interest is only mentioned. More detailed analytical procedures are given in Tanabe et al. (2023).

In-situ apatite U–Pb dating was also carried out with LA-ICP-MS at OUS. The measurement

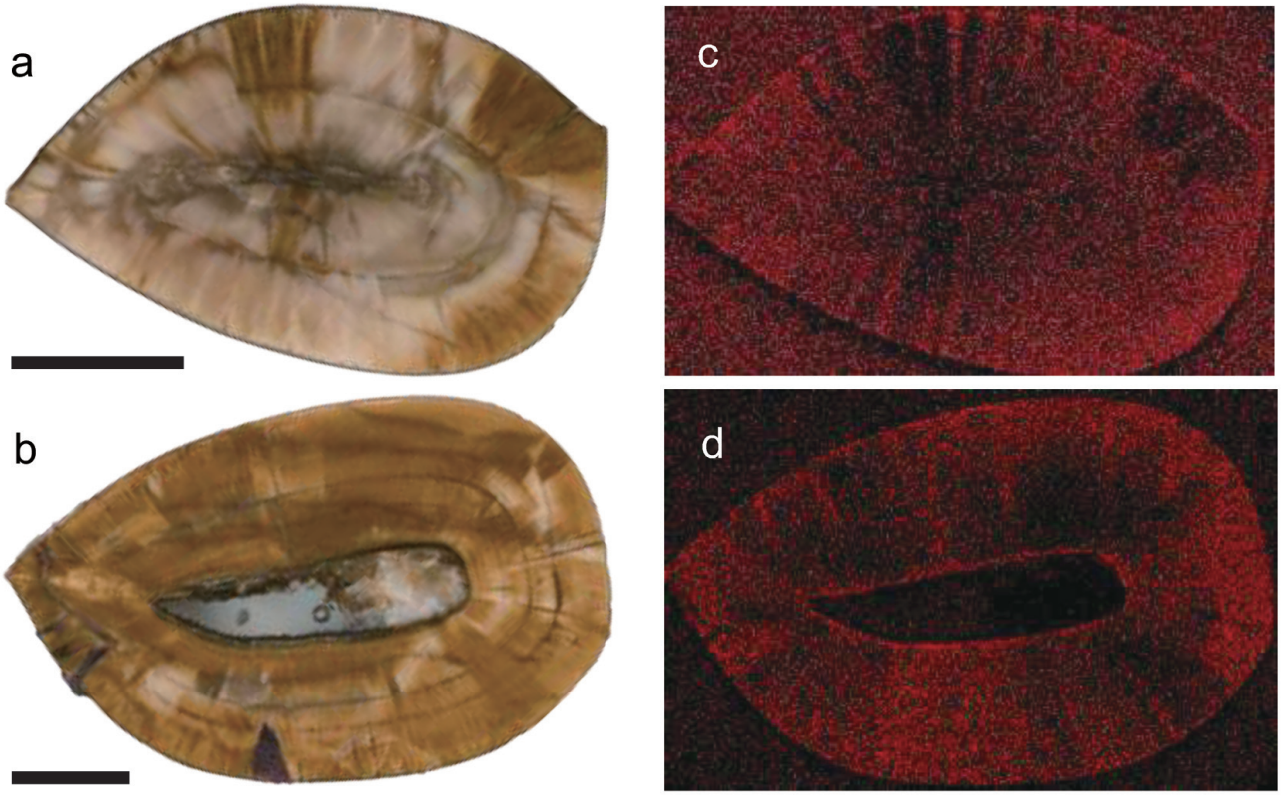

Fig. 2. Fossil teeth samples from *Tarbosaurus bataar* and the Y-images obtained by micro-XRF mapping. (a) Photographic image of MPC-D 100s/002. (b) Photographic image of MPC-D 100s/003. (c) Y-image of MPC-D 100s/002. (d) Y-image of MPC-D 100s/003. Scale bars equal 5 mm.

conditions were the same as those for the trace element analysis. The analyzed masses included six nuclides of ^{202}Hg, ^{204}Pb, ^{206}Pb, ^{207}Pb, ^{232}Th and ^{238}U. The background intensities were subtracted from the subsequent intensities at the ablation. OD306 apatite (Huang et al. 2015) and the 401 apatite (Thompson et al. 2016) were used as an external standard for the correction of the U/Pb ratios and as a secondary standard, respectively. Also, NIST SRM612 glass (Jochum et al. 2005) was analyzed as the external standard for the correction of the ^{207}Pb/^{206}Pb ratios. All uncertainties are quoted at a 2-sigma level. ^{235}U was calculated from ^{238}U using a ^{238}U/^{235}U ratio of 137.818 (Hiess et al. 2012). The apatite U–Pb age was calculated using Isoplot/Ex 4.15 (Ludwig 2012, and its update) based on the determination of a lower intercept age from the intersection of the Tera-Wasserburg (TW) concordia curve and a regression line from the data and anchored initial common Pb (Chew et al. 2011, Aoki et al. 2021). The initial common Pb isotopic ratio was assumed to be the terrestrial isotopic ratio provided by Stacey & Kramers (1975). The U–Pb analyses for the 401 (ca. 530 Ma) were conducted five times, and each analysis yielded the anchored-regression arrays (initial common Pb = 0.872) in a TW diagram with a lower intercept age of 523 ± 24 Ma. Further details of our apatite U–Pb analysis method are given in Tanabe et al. (2023).

IV. Results

1. MPC-D 100s/002

Figure 2c shows the areas with Y intensities, higher in red and lower in black, as obtained by the micro-XRF mapping. The mapping image suggests a heterogeneous distribution of regions with high and low Y concentrations, and a radial pattern of regions with high Y concentrations can be also observed. The trace element analysis demonstrates that the Y concentrations are 639–662 μg/g (N = 5) in the black regions and 886–951 μg/g (N = 5) in the red regions (Fig. 2c and Table 1). The U–Pb dating derived near the measurement points of the trace element analysis showed that the obtained ages from the black and red regions were 64.3 ± 3.4 Ma (N = 14, MSWD = 1.3) and 61.0 ± 11.0 Ma (N = 7, MSWD = 5.5), respectively (Fig. 3a, b). The fit of discordia model line was anchored at the common Pb ratio of the Late Cretaceous (0.842–0.840; Stacey & Kramers 1975).

2. MPC-D 100s/003

The red and black colors in Figure 2d obtained by the micro-XRF mapping measurement represent regions of relatively high and low Y intensities, indicating that the heterogeneous

Table 1. LA-ICP-MS apatite U–Pb and Y concentration data.

sample	Y-mapping area	U–Pb spot	$^{206}Pb/^{238}U$			$^{207}Pb/^{235}U$			Error correlation	$^{207}Pb/^{206}Pb$			Y* Spot	Y* µg/g
MPC-D 100s/002	black	1	0.13922	±	0.00407	15.00105	±	0.46336	0.94727	0.78182	±	0.00774	1	647
		2	0.14416	±	0.00422	15.58460	±	0.48138	0.94728	0.78443	±	0.00776	2	639
		3	0.15709	±	0.00460	17.15602	±	0.52992	0.94728	0.79242	±	0.00784	3	652
		4	0.15205	±	0.00445	16.76428	±	0.51784	0.94727	0.79999	±	0.00792	4	662
		5	0.16642	±	0.00487	18.10019	±	0.55909	0.94727	0.78919	±	0.00781	5	650
		6	0.15925	±	0.00466	17.45084	±	0.53905	0.94726	0.79509	±	0.00787		
		7	0.13406	±	0.00392	14.48197	±	0.44734	0.94726	0.78380	±	0.00776		
		8	0.14795	±	0.00433	16.04208	±	0.49551	0.94728	0.78674	±	0.00779		
		9	0.17282	±	0.00506	18.79964	±	0.58069	0.94729	0.78930	±	0.00781		
		10	0.15893	±	0.00465	17.21452	±	0.53171	0.94730	0.78592	±	0.00778		
		11	0.14497	±	0.00424	15.68358	±	0.48441	0.94731	0.78497	±	0.00777		
		12	0.15414	±	0.00451	16.67860	±	0.51517	0.94729	0.78513	±	0.00777		
		13	0.16482	±	0.00482	17.97960	±	0.55538	0.94726	0.79150	±	0.00783		
		14	0.15848	±	0.00464	17.37728	±	0.53676	0.94728	0.79561	±	0.00787		
	red	1	0.14750	±	0.00195	15.78579	±	0.23605	0.88616	0.77657	±	0.00538	1	888
		2	0.15209	±	0.00202	16.67009	±	0.24934	0.88605	0.79530	±	0.00551	2	950
		3	0.17816	±	0.00236	19.64616	±	0.29390	0.88603	0.80013	±	0.00555	3	951
		4	0.15970	±	0.00212	17.58242	±	0.26296	0.88612	0.79886	±	0.00554	4	886
		5	0.15612	±	0.00207	17.03023	±	0.25466	0.88620	0.79150	±	0.00548	5	932
		6	0.19314	±	0.00256	21.43334	±	0.32064	0.88606	0.80521	±	0.00558		
		7	0.16355	±	0.00217	17.99844	±	0.26920	0.88610	0.79849	±	0.00554		
MPC-D 100s/003	black	1	0.06007	±	0.00151	6.08589	±	0.16218	0.94079	0.73514	±	0.00664	1	558
		2	0.06345	±	0.00159	6.46418	±	0.17219	0.94103	0.73921	±	0.00666	2	529
		3	0.06034	±	0.00151	6.08561	±	0.16216	0.94083	0.73185	±	0.00661	3	548
		4	0.06271	±	0.00157	6.54318	±	0.17429	0.94107	0.75710	±	0.00682	4	558
		5	0.07665	±	0.00192	7.99702	±	0.21288	0.94147	0.75698	±	0.00679	5	516
		6	0.07092	±	0.00178	7.31245	±	0.19472	0.94125	0.74816	±	0.00673		
		7	0.06310	±	0.00158	6.46458	±	0.17223	0.94095	0.74334	±	0.00670		
		8	0.05863	±	0.00147	5.92526	±	0.15791	0.94074	0.73328	±	0.00663		
		9	0.06170	±	0.00155	6.21434	±	0.16564	0.94062	0.73081	±	0.00661		
		10	0.06471	±	0.00162	6.60038	±	0.17591	0.94070	0.74016	±	0.00669		
		11	0.06575	±	0.00165	6.76138	±	0.18014	0.94094	0.74621	±	0.00673		
		12	0.06852	±	0.00172	7.02200	±	0.18707	0.94096	0.74358	±	0.00671		
	red	1	0.10112	±	0.00135	10.85230	±	0.16425	0.87979	0.77874	±	0.00560	1	1752
		2	0.10260	±	0.00137	10.83941	±	0.16390	0.88025	0.76660	±	0.00550	2	1783
		3	0.10263	±	0.00137	10.95622	±	0.16560	0.88047	0.77460	±	0.00555	3	1833
		4	0.10737	±	0.00143	11.57125	±	0.17482	0.88076	0.78195	±	0.00559	4	1819
		5	0.09889	±	0.00132	10.48777	±	0.15862	0.88013	0.76950	±	0.00552	5	1775
		6	0.10257	±	0.00136	10.86839	±	0.16425	0.88052	0.76887	±	0.00551		
		7	0.10065	±	0.00134	10.57520	±	0.16017	0.87938	0.76234	±	0.00550		

*Measured at a point close to the U-Pb measurement point

and radial Y distributions are similar to MPC-D 100s/002 (Fig. 2c). The Y concentration of 516–558 µg/g (N = 5) and 1752–1833 µg/g (N = 5) were obtained from the black and red regions in Figure 2d, respectively (Table 1). The U–Pb ages obtained from the model line anchored at the terrestrial isotopic ratio of the Late Cretaceous (Stacey & Kramers 1975) were 51.5 ± 2.7 Ma (N = 12, MSWD = 3.0) from the black region (Fig. 3c) and 57.3 ± 6.1 Ma (N = 7, MSWD = 4.7) from the red regions (Fig. 3d).

V. Discussion and Conclusion

In MPC-D 100s/002, the U–Pb age (64.3 ± 3.4 Ma) from the region with low Y concentration is congruent with the age of this sample reported in the previous study (66.7 ± 2.5 Ma; Tanabe et al. 2023). The Y concentrations between the regions where the two ages were derived do not differ significantly (639–662 µg/g and 338–589 µg/g). The age of 61.0 ± 11.0 Ma obtained from the region with relatively high Y concentration (Y = 886–951 µg/g) is younger than the above ages, but older than 34.7 ± 3.3 Ma, which is obtained from a higher Y concentration region (819–1226 µg/g; Tanabe et al. 2023). These comparisons indicate that the Y concentration correlates with the obtained U–Pb ages and that the ages in areas with lower Y concentrations tend to show older ages, which is consistent with the results of Greene et al. (2018) and Tanabe et al. (2023). In MPC-D 100s/003, the U–Pb age of 51.0 ± 2.7 Ma was obtained from the low Y

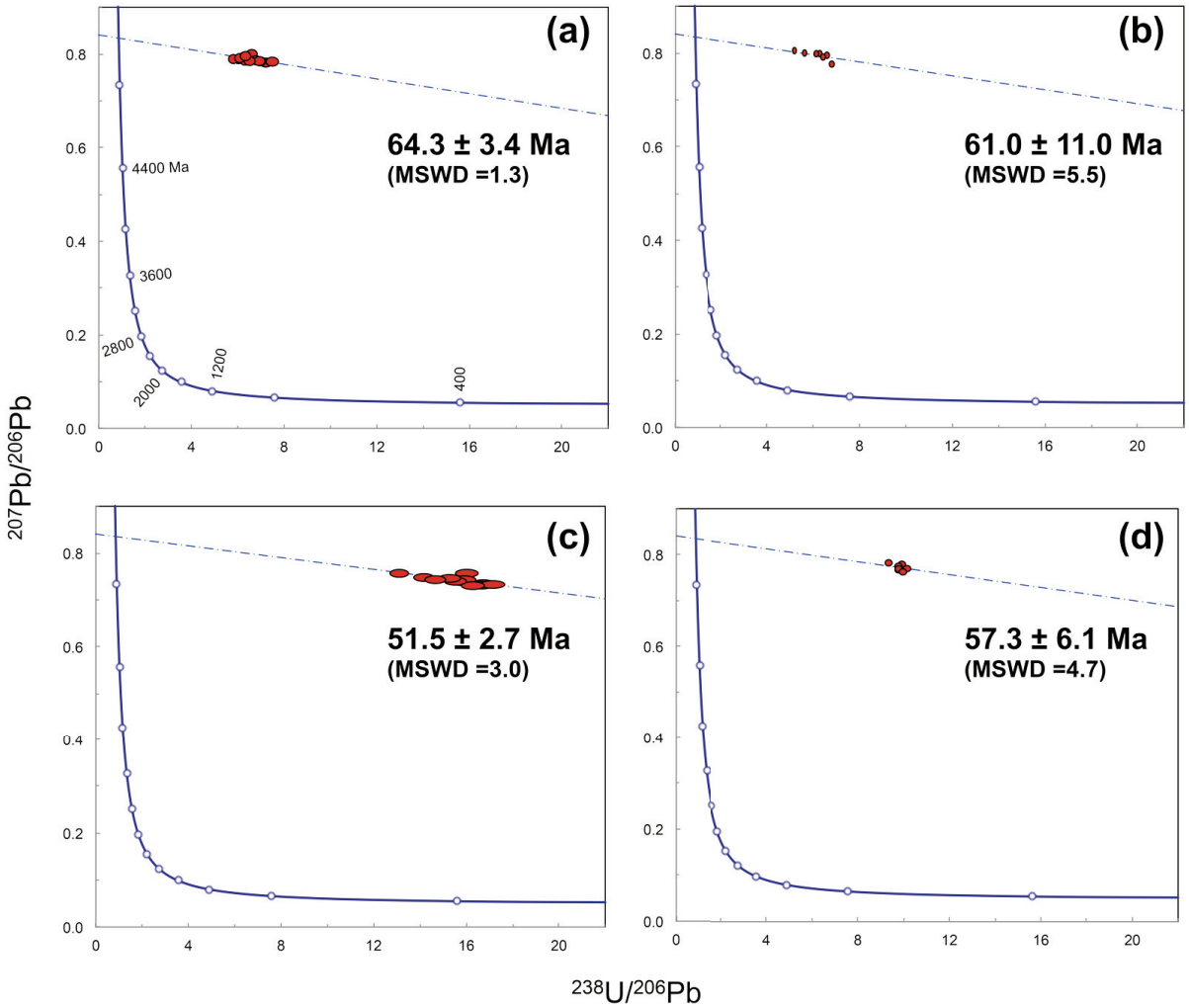

Fig. 3. Tera–Wasserberg diagram of apatite analyses with an error bar (2 sigma). (a) Black region of MPC-D 100s/002. (b) Red region of MPC-D 100s/002. (c) Black region of MPC-D 100s/003. (d) Red region of MPC-D 100s/003.

concentration region (516–558 μg/g) and 56.6 ± 6.1 Ma from the high Y concentration region (1752–1833 μg/g). Tanabe et al. (2023) obtained even younger ages (28.0 ± 4.6 Ma and 33.7 ± 2.2 Ma) from the areas with higher Y concentrations in this sample (962–2595 μg/g and 1107–2051 μg/g, respectively). This trend is consistent with the correlation between the U–Pb age and the Y concentration in the MPC-D 100s/002. The results in this study and data from Tanabe et al. (2023) indicate that Y concentrations can be a qualitative indicator of post-fossilization alteration for apatite U–Pb dating. The regions with relatively high concentrations of Y have been strongly affected by post-fossilization alteration and show younger U–Pb ages compared to the relatively low Y concentration regions within the sample.

Although consideration of Y concentrations can be beneficial for apatite U–Pb dating, we should not overlook the fact that it is impossible to set the universal quantitative threshold of Y concentration to distinguish the ideal regions for obtaining the fossilization age since our data indicates the values and variation in the Y concentration varies depending on samples. When the data are lumped together using the MPC-D 100s/002 and 100s/003 as the same sample, the correlation between the Y concentration and the U–Pb age mentioned above cannot be confirmed. Therefore, it should be noted that the Y-screening method requires comparing Y concentrations only within the same sample.

This study reconfirms that it would be desirable to selectively measure regions of samples with the lowest Y concentration to obtain geologically meaningful fossilization ages by apatite U–Pb dating. The range of Y was measured by sequential spot analyses along linear transects in each sample in Greene et al. (2018) to visualize the trend of Y distribution from the inside to the outside of the samples. Depending on the sample, it would be difficult to capture the general spatial trend of the Y distribution in a single linear transaction. Contrarily, the maps shown in this study (Fig. 2c, d) can non-destructively visualize the

Y distribution of the whole sampling area in 2D. This study clearly demonstrates that Y mapping using micro-XRF is a powerful technique for quick visualization of relative differences in the effects of post-fossilization alteration within a fossil tooth sample.

We would like to note that the apatite U–Pb dating of tooth samples is easily affected by post-fossilization alteration, and therefore, the age estimate can only be used as a lower limit of the fossilization age (Tanabe et al. 2023). The apatite U–Pb dating combined with the Y-screening method alone cannot determine a geologically meaningful age, but the apatite U–Pb age combined with existing and reliable ages from other lines of evidence (e.g., biostratigraphic data and U–Pb ages from igneous rocks and caliches) could provide important supporting data to constrain the depositional ages of fossil-bearing strata and the temporal range of the yielded fossil remains. In conclusion, we have found that the Y micro-XRF mapping is a useful tool for non-destructive visualization of the effect of post-fossilization alteration in fossil teeth and for selecting preferable measuring points for LA-ICP-MS apatite U–Pb dating.

Acknowledgements

We are grateful to M. Tanabe and S. Miyake for their support in data collection, N. Shimobayashi for his support in micro-XRF mapping, and K. Brink for editorial assistance. We also thank two anonymous reviewers for their helpful comments. This study was financially supported by JSPS KAKENHI Grant Number JP19K04043 (K.A.).

References

Aoki, S., Date, Y., Nishido, H. & Aoki, K. (2021) LA-ICP-MS U–Pb dating of the 401 apatite. *Naturalistae* 25: 23-27.

Barreto, A. M. F., Bertotti, A. L., Sylvester, P. J., Prado, L. A. C. do, Araripe, R. C., Oliveira, D. H. de, Tomé, M. E. T. R., Lemos, F. A. P., Nascimento, L. R. L. do, Pereira, P. A. & Albayrak, A. I. (2022) U/Pb geochronology of fossil fish dentine from Romualdo Formation, Araripe Basin, northeast of Brazil. Journal of South American Earth Sciences 116: 103774.

Brusatte, S. L., Carr, T. D. & Norell, M. A. (2012) The Osteology of *Alioramus*, a gracile and long-snouted tyrannosaurid (Dinosauria: Theropoda) from the Late Cretaceous of Mongolia. Bulletin of the American Museum of Natural History 366: 1-197.

Chew, D. M., Babechuk, M. G., Cogné, N., Mark, C., O'Sullivan, G. J., Henrichs, I. A., Doepke, D. & McKenna, C. A. (2016) (LA,Q)-ICPMS trace-element analyses of Durango and McClure Mountain apatite and implications for making natural LA-ICPMS mineral standards. Chemical Geology 435: 35-48.

Eberth, D. A. (2018) Stratigraphy and paleoenvironmental evolution of the dinosaur-rich Baruungoyot-Nemegt succession (Upper Cretaceous), Nemegt Basin, southern Mongolia. Palaeogeography, Palaeoclimatology, Palaeoecology 494: 29-50.

Fassett, J. E., Heaman, L. M. & Simonetti, A. (2011) Direct U-Pb dating of Cretaceous and Paleocene dinosaur bones, San Juan Basin, New Mexico. Geology 39(2): 159-162.

Greene, S., Heaman, L. M., DuFrane, S. A., Williamson, T. & Currie, P. J. (2018) Introducing a geochemical screen to identify geologically meaningful U-Pb dates in fossil teeth. Chemical Geology 493: 1-15.

Hiess, J., Condon, D. J., McLean, N. & Noble, S. R. (2012) $^{238}U/^{235}U$ Systematics in Terrestrial Uranium-Bearing Minerals. Science 335(6076): 1610-1614.

Huang, Q., Kamenetsky, V. S., McPhie, J., Ehrig, K., Meffre, S., Maas, R., Thompson, J., Kamenetsky, M., Chambefort, I., Apukhtina, O. & Hu, Y. (2015) Neoproterozoic (ca. 820–830Ma) mafic dykes at Olympic Dam, South Australia: Links with the Gairdner Large Igneous Province. Precambrian Research 271: 160-172.

Ishigaki, S., Tsogtbaatar, K., Toyoda, S., Mainbayar, B., Noumi, Y., Takahashi, A., Buyantegsh, B., Byambaa, P., Zorig, E., Bayardorj, C., Ochirjantsan, E., Saneyoshi, M., Hayashi, S. & Chiba, K. (2018) Report of the Okayama University of Science – Mongolian Institute of Paleontology Joint Expedition in 2018. Bulletin of Research Institute of Natural Science, Okayama University of Science 44: 19-32.

Jerzykiewicz, T. & Russell, D. A. (1991) Late Mesozoic stratigraphy and vertebrates of the Gobi Basin. Cretaceous Research 12(4): 345-377.

Jochum, K. P., Pfänder, J., Woodhead, J. D., Willbold, M., Stoll, B., Herwig, K., Amini, M., Abouchami, W. & Hofmann, A. W. (2005) MPI-DING glasses: New geological reference materials for in situ Pb isotope analysis. Geochemistry, Geophysics, Geosystems 6: 1525-2027.

Kocsis, L., Trueman, C. N. & Palmer, M. R. (2010) Protracted diagenetic alteration of REE contents in fossil bioapatites: Direct evidence from Lu–Hf isotope systematics. Geochimica et Cosmochimica Acta, 74(21): 6077-6092.

Kurumada, Y., Aoki, S., Aoki, K., Kato, D., Saneyoshi, M., Tsogtbaatar, K., Windley, B. F. & Ishigaki, S. (2020) Calcite U–Pb age of the Cretaceous vertebrate-bearing Bayn Shire Formation in the Eastern Gobi Desert of Mongolia: usefulness of caliche for age determination. Terra Nova 32: 246-252.

Machida, S., Nakamura, K., Kogiso, T., Shimomura, R., Horinouchi, K., Okino, K. & Kato, Y. (2021) Fine-scale chemostratigraphy of cross-sectioned hydrogenous ferromanganese nodules from the western North Pacific. Island Arc 30(1): e12395.

Ludwig, K. R. (2012) User's manual for Isoplot 3.75, revised 30 January, 2012. Berkeley Geochronology Center, Special Publication, 5.

Romer, R. L. (2001) Isotopically heterogeneous initial Pb and continuous ^{222}Rn loss in fossils: The U-Pb systematics of *Brachiosaurus brancai*. Geochimica et Cosmochimica Acta, 65(22): 4201-4213.

Stacey, J. S. & Kramers, J. D. (1975) Approximation of terrestrial lead isotope evolution by a two-stage model. Earth and Planetary Science Letters 26(2): 207-221.

Tanabe, M., Aoki, K., Chiba, K., Saneyoshi, M., Kodaira, S., Nishido, H., Mainbayar, B., Tsogtbaatar, K. & Ishigaki, S. (2023) Apatite U–Pb dating of dinosaur teeth from the Upper Cretaceous Nemegt Formation in the Gobi Desert, Mongolia: contribution to depositional age constraints. Island Arc 32(1): e12488.

Thompson, J., Meffre, S., Maas, R., Kamenetsky, V., Kamenetsky, M., Goemann, K., Ehrig, K. & Danyushevsky, L. (2016) Matrix effects in Pb/U measurements during LA-ICP-MS analysis of the mineral apatite. Journal of Analytical Atomic Spectrometry 31(6): 1206-1215.

青木一勝・千葉謙太郎・小木曽哲・村上凱星・TSOGTBAATAR Khishigjav：アパタイトU–Pb年代測定のためのマイクロXRFによる歯化石のイットリウムマッピング

要約

歯化石のアパタイトU–Pb年代測定では，化石化後の変質の影響の少ない測定試料／測定箇所を選定することが重要である．先行研究から同一試料内におけるイットリウムの濃度の違いが，定性的な変質の指標として有効であることが示唆されている．本研究ではその有用性を検証するため，既に年代値が報告されているタルボサウルスの歯化石２試料に対し，マイクロ蛍光X線分析装置を使ったイットリウムのマッピング測定から測定領域を選定し，LA-ICP-MSアパタイトU–Pb年代測定を行った．その結果，先行研究で 66.7 ± 2.5 Ma の年代値が報告された試料からは，イットリウム濃度が相対的に異なる２つの領域からそれぞれ 64.3 ± 3.4 Ma と 61.0 ± 11.0 Ma の年代値が得られた．また，約30 Ma の年代値を示した試料からは 51.5 ± 2.7 Ma と 57.3 ± 6.1 Ma の年代値が得られた．これらの結果は少なくとも同一試料内では，イットリウム濃度とアパタイトU–Pb年代値に定性的な相関があることを示す．さらなる検証は必要ではあるが，マイクロ蛍光X線分析装置マッピング測定が歯化石の変質の程度を非破壊で視覚化する手法として有効であり，アパタイトU–Pb年代測定における測定点の選定に利用できるだろう．

(Accepted 5 November 2023)